Measuring and Modeling the Kinetics of Individual DNA–DNA Polymerase Complexes on a Nanopore

Hongyun Wang,[†] Nicholas Hurt,[‡] and William B. Dunbar[§,*]

[†]Department of Applied Mathematics and Statistics, [‡]Department of Chemistry and Biochemistry, and [§]Department of Computer Engineering, University of California, Santa Cruz, California 95064, United States

ABSTRACT The assembly of a DNA–DNA polymerase binary complex is the precursory step in genome replication, in which the enzyme binds to the 3′ junction created when a primer binds to its complementary substrate. In this study, we use an active control method for observing the binding interaction between Klenow fragment (exo-) (KF) in the bulk-phase chamber above an α-hemolysin (α-HL) nanopore and a single DNA molecule tethered noncovalently in the nanopore. Specifically, the control method regulates the temporal availability of the primer-template DNA to KF binding and unbinding above the nanopore, on millisecond-to-second time scales. Our nanopore measurements support a model that incorporates two mutually exclusive binding states of KF to DNA at the primer-template junction site, termed "weakly bound" and "strongly bound" states. The composite binding affinity constant, the equilibrium constant between the weak and strong states, and the unbound-to-strong association rate are quantified from the data using derived modeling analysis. The results support that the strong state is in the nucleotide incorporation pathway, consistent with other nanopore assays. Surprisingly, the measured unbound-to-strong association process does not fit a model that admits binding of only free (unbound) KF to the tethered DNA but does fit an association rate that is proportional to the total (unbound and DNA-bound) KF concentration in the chamber above the nanopore. Our method provides a tool for measuring pre-equilibrium kinetics one molecule at a time, serially and for tens of thousands of single-molecule events, and can be used for other polynucleotide-binding enzymes.

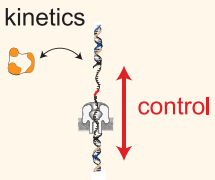

KEYWORDS: active control of DNA · nanopore · α-hemolysin · Klenow fragment · single molecule · modeling kinetics

The DNA polymerases catalyze the incorporation of deoxyribonucleotides into DNA during genome replication and are the greatest contributors to the high accuracy of this process.[1] The nucleotide incorporation cycle is initiated when the enzyme binds to a template that has been primed, thereby forming a binary protein/DNA complex. Subsequently, the enzyme preferentially incorporates deoxyribonucleoside triphosphates (dNTPs) that are complementary to the template strand. The sequential progression through a series of kinetic checkpoints en route to forming an activated ternary complex that is competent for phosphodiester bond formation prevents the incorporation of incorrectly paired dNTPs.[2] To increase fidelity, the polymerase will sample different conformations, and those most conducive to correct dNTP incorporation are chosen. Crystal structures of family A polymerases show a conserved polymerase domain that resembles a right hand, with three principle subdomains termed palm, fingers, and thumb.[1] The palm subdomain connects the thumb and fingers subdomains, with an interior surface that contains the enzymatic active site and bears amino acids essential for catalysis. The thumb subdomain binds the DNA substrate and facilitates positioning of the primer/template duplex at the active site, while the fingers subdomain binds incoming dNTPs. By rotating a portion of the finger subdomain to form a stable fingers-closed ternary complex, an incoming dNTP is positioned toward the active site, now in position for phospodiester bond forming chemistry to proceed.

This paper examines the assembly kinetics between the Klenow fragment (exo-) of *Escherichia coli* DNA polymerase I (KF) with the 3′ end of the primer/DNA interface. A variety of ensemble measurement techniques have been used to establish and measure KF kinetics and checkpoints, including rapid quench-flow methods to quantify steady-state and pre-steady-state kinetics[3,4] and stopped-flow fluorescence[5] and fluorescence resonance energy transfer (FRET)[6]

* Address correspondence to dunbar@soe.ucsc.edu.

Received for review October 13, 2012 and accepted April 5, 2013.

Published online April 08, 2013
10.1021/nn401180j

to identify checkpoints and their positions on the selection pathway. The checkpoints for base and sugar recognition occur after the initial binding of a nucleotide to the enzyme, and the binary KF/DNA complex is, preferentially, in a "fingers-open" configuration to receive the incoming nucleotide. Although the initial expectation based on crystallographic data was that the KF–DNA binary complex would be exclusively in the open configuration, a recent study using single-molecule FRET (smFRET) showed that the fingers-closed conformation is sampled for a significant subpopulation of binary complexes (~34% in the study).[7] In the same study, the transition time scales between open *versus* closed conformations of individual KF were estimated to have rapid (≤3 ms) transitions for unliganded KF and longer (>10 ms) transitions for binary complexes. Biological nanopores have been used to measure millisecond time scale transitions between binary and ternary complexes (in the presence of dNTPs) at the single-molecule level.[8−10] Nanopores, which can only measure KF when complexed with DNA, have not been able to discriminate between open and closed binary configurations, though it has been shown that both open binary and closed ternary configurations are sampled on the nanopore in the presence of complementary dNTPs.[9] In this paper, we examine the kinetics of binary complex assembly (absent dNTP substrate) using mathematical modeling and a novel single-molecule measurement technique that combines a nanopore with active control. The control technique is an extension of our previous method[11] and is the first to permit direct electrical measurement of association and unforced dissociation between KF and DNA, one molecule at a time.

Biological nanopores provide a simple method of analyzing populations of DNA and enzyme-bound DNA molecules, by serially capturing and measuring one complex at a time.[12] The heptameric protein α-hemolysin (α-HL) is an asymmetric membrane-spanning pore characterized by an expanded vestibule at one end (*cis*-chamber side) that tapers to a limiting 1.5 nm diameter aperture (lumen), which is just wide enough to accommodate single-stranded DNA (ssDNA).[13] Beyond the lumen, the stem extends to the *trans*-chamber side. Using a sensitive voltage-clamp amplifier, the device monitors ionic current through the pore (Figure 1a). Open channel current through the α-HL pore is ~60 pA at 180 mV applied potential in 0.3 M KCl (Figure 1b). The field force exerted on the negatively charged backbone results in the capture of individual DNA molecules into the nanopore from the bulk-phase *cis*-chamber, with each molecule causing a current blockade of finite duration. The change in duration and mean amplitude of the current levels caused by these blockages are used to characterize the "events" in nanopore experiments. With primer-bound template substrate alone in the *cis*-chamber, capture of

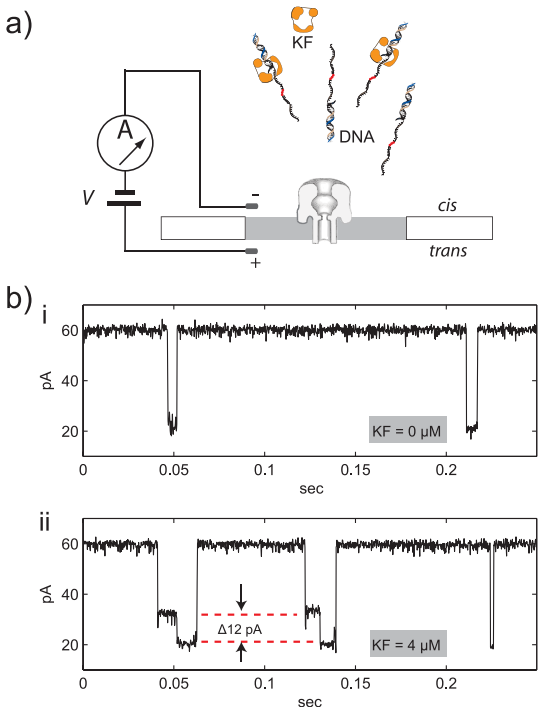

Figure 1. Detection of DNA capture events using a nanopore. (a) A patch-clamp amplifier supplies voltage and measures ionic (KCl) current through a single α-hemolysin channel. DNA and KF molecules are in the *cis*-chamber above the pore. (b) Example current recordings at 180 mV in 0.3 M KCl, with 1 μM DNA in the *cis*-chamber, and (i) KF = 0 and (ii) KF = 4 μM concentrations in the *cis*-chamber. Open channel current is 60 pA. Current reduction events register capture of individual DNA molecules into the nanopore, with each event characterized by the attenuated amplitude of finite duration. (i) Absent KF, capture events show a single-level amplitude (22 pA). (ii) Addition of KF results in a new two-level event type, characterized by a 12 pA transition from a higher (34 pA) to a lower (22 pA) level. Single-level events at 22 pA are also observed.

each DNA at the single-stranded end is revealed by a single-level blockade (22 pA, Figure 1b,i). The duration of these events, known as the "dwell time", represents the time required for the applied voltage to dissociate the duplexed DNA, resulting in the subsequent passage of both strands independently into the *trans*-chamber; this results in a return to the open channel current.[8] When DNA and KF are substrates in the *cis*-chamber, two event types are observed (Figure 1b,ii): single-level amplitude events comparable to those in the DNA alone experiments (22 pA), and two-level events characterized by an initial 34 pA amplitude that transitions to an amplitude of 22 pA. One aim of our study is to infer the potential interactions between KF and DNA that cause these two event types.

Our objective is to model the pre-equilibrium kinetics between the KF and DNA substrate, based on capture event measurements (Figure 1), and using affinity measurements of an individual KF for a single DNA controlled in the nanopore. This study is the first to show that KF–DNA complexes captured on the pore are not universally detectable. Specifically, through

extensive experimentation and logical reasoning, we show that capture events that register a pattern consistent with unbound DNA (with the pattern being established in experiments absent KF, Figure 1b,i) can also register for binary complexes where the enzyme is too labile to survive the initial contact force with the nanopore upon capture and is "knocked-off". Our results show that two-level events (Figure 1b,ii) are due to KF/DNA complex formation that only partially impedes channel conductance when captured, and only after KF dissociation does full current attenuation occur, which is relieved by passing the two DNA strands independently. Additionally, our study complements prior nanopore studies on KF−DNA kinetics[9,10] by measuring and quantifying the rates of formation of binary complexes.

RESULTS AND DISCUSSION

We sought to identify what KF/DNA complexes can be captured on the nanopore by classifying the two event types present when performing capture experiments involving both KF and DNA in the *cis*-chamber (Figure 1b,ii). To classify each event type, we established criteria for events that occur in the absence (type A) or presence (type B) of KF. Due to day-to-day variations and imperfections in the nanopore experiment, the two event types cannot be perfectly identified. An event is assigned type B if it has two levels with an amplitude difference of at least 3 pA and a first level (pretransition) amplitude above 29 pA; otherwise, it is assigned type A. We computed the average amplitude and dwell time of each event, based on the pretransition signal for type B events and based on the full event signal for type A events. We then plotted these average amplitude *versus* dwell times, first in experiments with only 1 μM DNA in the *cis*-chamber and without KF (Figure 2a,i). From three experiments repeated on different days, 1004 events were assigned type A and six were assigned type B, meaning 0.6% of type A events being misidentified as type B (false positives) in the absence of KF. Next, with 1 μM DNA and 1 μM KF added to the *cis*-chamber in two separate experiments, 298 events were assigned type A with 396 assigned type B (57.1%, Figure 2a,ii). Histograms of the computed event amplitudes show that the events assigned type A and type B are well-separated in the dimension of average amplitude (Figure 2b). The choice of 29 pA as the pretransition amplitude for assigning type B events provides an acceptable trade-off between minimizing false positives without appreciably cutting into the amplitude distribution of type B events. An amplitude histogram of the difference between the pre- and post-transition average in type B events (Figure 2b, inset) also validates the choice of 3 pA as the minimum transition size for assigning type B, with a negligible fraction of false negatives (type B events having <3 pA steps). A statistical analysis that further justifies our choice of criteria for classifying events as type A or B is provided in Supporting Information (Figure S2).

After establishing criteria to classify the two event types, we wanted to correlate the nanopore KF/DNA captured complex to event type. Since type B events are present only with KF and DNA, they correspond to KF bound in some state to the captured DNA. Conversely, type A events are present with and without KF present. Therefore, type A events correspond to either unbound DNA or KF bound to DNA in a configuration that is different from that corresponding to type B events. In such a case, KF would be bound to DNA in a state that is too labile to survive the initial contact force with the nanopore upon capture, thus registering as an event that is indistinguishable from unbound DNA. To test whether KF-bound DNA can cause type A events, we examined the percentage of type B events at saturating KF concentration. Under these conditions, if the detectable binding state that causes type B events is the only KF-binding state, then the fraction of type B events should go to near 100%. In fact, the percentage of type B events does not approach 100% at saturating KF concentration, but settles at ~65% (Figure 3a).

To test the validity of this result, we considered the possibility that our experimental method was the reason the observed percentage of type B events saturates well below 100%; that is, although 65% are measured type B, 100% are type B in the bulk phase. In that case, a candidate explanation is that the unobserved ~35% is caused by type B events with a pretransition signal that is too fast to be observed with the nanopore. The lifetime of pretransition signals has a single-exponential distribution (Figure S3), which supports the assertion that dissociation of KF from DNA in this state is dominated by a single kinetic transition. Though our instrument cannot resolve pretransition signals faster than 0.2 ms, the exponential distribution with mean 6.8 ms of the pretransition duration allows us to calculate the percentage of the missed pretransition signals (ones faster than 0.2 ms). On the basis of that calculation, we determine a correction factor of $\eta = 1.03$, where the true percentage is η times the observed percentage (Supporting Information). Thus, the unobserved 35% cannot be attributed to type B events too fast for detection. Next, we considered whether the measured type B percentage reflects the true fraction of type B complexes in the bulk-phase *cis*-chamber. To test this, the capture rate of type A events alone (absent KF) was compared to the capture rate of type A and B events together (at saturating KF). These rates were statistically indistinguishable (Figure S4), suggesting that the measured fraction represents the fraction in the bulk-phase *cis*-chamber. We considered next that the observed value of only 65% when KF is saturating is caused by an incomplete hybridization of the primer

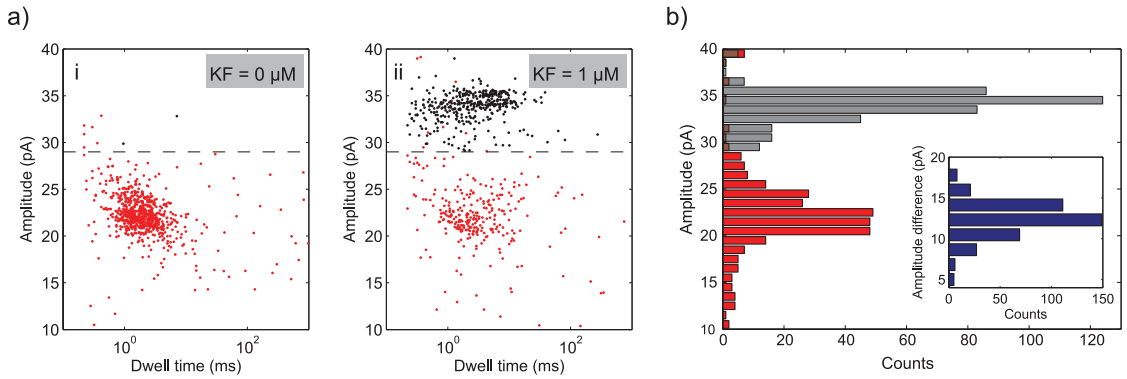

Figure 2. Identifying and classifying event types in experiments with DNA, with and without KF. (a) Event plots show the mean amplitude and dwell time for each capture event, using the pretransition signal for type B events (black) and the full event signal for type A events (red). (i) With 1 μM DNA in the *cis*-chamber and without KF, 99.4% of 1006 events are assigned type A. (ii) Adding 1 μM KF in the *cis*-chamber, 42.9% of 667 events are assigned type A. (b) From experiments with DNA and KF (a,ii), the event amplitude histograms of type A events (red, 22.7 $\pm$ 5.2 pA) and type B events (gray, 34.0 $\pm$ 1.8 pA) show a separation in the distributions. Inset: Amplitude difference histogram for type B events shows the distribution of transition step sizes (12.4 $\pm$ 2.1 pA), well above the 3 pA minimum used to assign type B events.

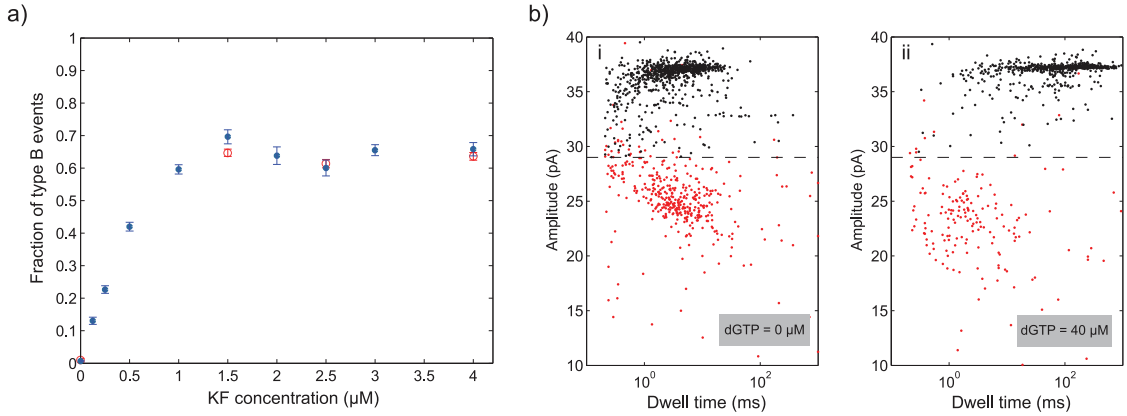

Figure 3. Two KF−DNA binding configurations are captured, but only one is detectable. (a) With 1 μM DNA in the *cis*-chamber, the fraction of type B events saturates with increasing KF concentration, suggesting two mutually exclusive binary configurations with one corresponding to type B events. The data points are $p = M/N$ with M type B events out of N total events, with standard error $(p(1 - p)/N)^{1/2}$. Doubling the primer concentration for a 2:1 primer-template ratio (red open circles) assures that all templates are hybridized and did not affect the fraction at saturation. (b) Event plots show the mean amplitude and dwell time for each capture event (i) without and (ii) with complementary dNTP (40 μM dGTP), with 1 μM DNA and 4 μM KF in the *cis*-chamber. The plots show that the binary configuration that corresponds to type B events is stabilized by dGTP, indicated by an increase in the fraction of type B events ((i) 68% of 1253 events, (ii) 79% of 818 events) and their mean duration ((i) 6.8 ms and (ii) 163.3 ms). Pretransition amplitudes were conserved: (i) 36.3 $\pm$ 1.8 pA, and (ii) 36.9 $\pm$ 1.2 pA.

with template DNA when added to the *cis*-chamber. To test this, we doubled the primer concentration to ensure hybridization goes to 100%. The same saturation at ~65% is observed with 2:1 primer-template ratio (Figure 3a, red data), suggesting that incomplete duplex formation is not the reason for the 35% of type A events when KF is saturating.

Another candidate explanation for saturation below 100% is that a significant subpopulation of the enzyme is "crippled" and does not bind to DNA. As a potential source for this, we considered the possibility that the addition of glycerol, which accompanies each addition of KF to the *cis*-chamber, causes a substantial fraction of KF to remain inert. When glycerol concentration at 1.5 μM KF is doubled, the fraction of type B events was conserved at 64% (out of 2397 total events), suggesting that the glycerol does not inhibit KF binding. In any case, even if a significant subpopulation of the enzyme was inert, the fraction of type B events would still increase or decrease if the glycerol effect is greater than the effect of additional enzyme, but it would not plateau. To further show that the KF stock used is competent for binding, we added 40 μM complementary dNTP (dGTP) to the *cis*-chamber, with 1 μM DNA and 4 μM KF present. A 3′-H-terminated primer is used in all results shown, which prevents catalytic turnover. The result was an increase in the fraction of type B events (from 68 to 79%) and a dramatic increase in the lifetime of pretransition signals of type B events (from 6.8 to 163.3 ms mean) while maintaining the same pretransition amplitude (Figure 3b). This suggests that dGTP stabilizes the

configuration that corresponds to type B events, yet does not change the complex enough to generate a different amplitude signature. To connote a KF binding state that can be stabilized by complementary dNTP, we henceforth refer to the type B binding configuration as the "strong binding state".

The results above support the existence of a binding state (or states) between KF and captured DNA that register as type A events, and to contrast this with type B events, we term the state the "weak binding state". The weak and strong states are mutually exclusive; that is, the weakly bound complex prevents the DNA from forming the strong state with another KF molecule in bulk solution, and vice versa. If the weak and strong state were not exclusive, a gradual increase in detectably bound (strong state) complexes would be observed as KF concentration increases. To reaffirm the existence of the strong and weak states, we repeated the experiments on different nanopore workstations, by a different experimenter, and using different syntheses of DNA, and all results yielded the same trend (Table S1). Collectively, our results support that the weak and strong states are distinct and exclusive configurations and intrinsic to the KF−DNA binary complexes that can be captured on the nanopore.

There is precedent for the molecular identify of the strong state in the nanopore literature. In the first study,[8] the pretransition duration was identified as the lifetime of the KF−DNA complex, while the subsequent second-level duration was identified as the dwell time of unbound DNA, following voltage-promoted dissociation of KF from the DNA. Then in ref 9, it was shown that complementary dNTP can repeatedly bind and unbind to the strong-state complex while residing on top of the pore under voltage force. Iterative dNTP binding and unbinding was revealed as an increase in first-level duration as dNTP concentration was increased (as in Figure 3b,ii). While the binary (KF/DNA) and ternary (KF/DNA/dNTP) complexes can be distinguished based on their dwell time at sufficient concentrations of complementary dNTP, these complexes could not be distinguished based on the measured current amplitude (as in Figure 3b,i-ii). More recently, though, amplification of the two-level amplitude difference by use of abasic residues in the template strand has permitted detection of a 1 pA difference in pretransition amplitudes between binary and ternary complexes with complementary dNTP.[10] Amazingly, the current difference corresponds to a shift of less than 1 nucleotide in the template strand position in the pore lumen. Although the binary complex samples the fingers-open state on the nanopore,[9] it remains unknown if the binary complex samples the fingers-closed state on the nanopore at voltages that are large enough to promote capture into the nanopore (>100 mV in 0.3 M KCl). Since smFRET showed that the binary complex samples the open and closed states absent force,[7] we suspect that the open and closed binary complex would be present in the first-level amplitude of two-level events at *sufficiently low voltage force*. However, low voltage deteriorates capture rate and the signal used to detect complex-induced changes in current amplitude, making amplitude-based differentiation of open *versus* closed binary complex on the pore highly unlikely. While the open configuration registers as the strong state (by accommodating dNTP incorporation as in ref 9), we do not know if the strong state also samples the closed binary configuration at the high voltages used here to promote DNA capture. In capture experiments, a single kinetic transition is observed in the strong-state lifetime distribution (Figure S3). If the strong state does sample the closed binary configuration, then the observed single kinetic transition implies that either the strong-state has the same dissociation rate for the closed configuration as for the open configuration or the closed configuration and the open configuration are in fast equilibrium.

We have not established a molecular identity for the weak state, and more than one configuration could be contributing to the weak state population. A candidate configuration for the weak state is KF binding to the blunt end. To test this, we replaced the linear DNA duplex formed by primer-template annealing with a hairpin structure in which the complementary template and primer strand were linked *via* a stable tetraloop, while conserving the sequence. In a FRET-based study of KF,[6] the hairpin structure was used to replace linear DNA duplex to eliminate the possibility of the polymerase binding to the opposite (blunt) end. No increase in the fraction of strong state events at saturating KF concentration was observed with the hairpin DNA (Figure S5), suggesting that blunt-end binding of KF to the linear DNA duplex is not appreciably present and cannot therefore be the source of the observed weak state population. Alternatively, the weak state could be the DNA bound to KF at the exonuclease site. Specifically, although the KF used in our experiments is deficient in 3′−5′ exonuclease activity (D355A,E357A mutant), this does not preclude the possibility that for a fraction of the complexes the primer strand has been transferred to the exonuclease active site.[14] The resulting exo-site-bound DNA would produce a complex that would mutually exclude KF binding to the polymerase active site. Moreover, though the mutant protein significantly reduces the abundance of DNA bound to the exonuclease site compared to the wild-type protein, exonuclease site binding is not completely eliminated. Still another possibility is that the weak state is the closed binary complex with KF at the polymerase active site, which is known to be the less dominant of the two configurations (open *vs* closed) absent contact force.[7] Other candidate configurations are possible. Though we do

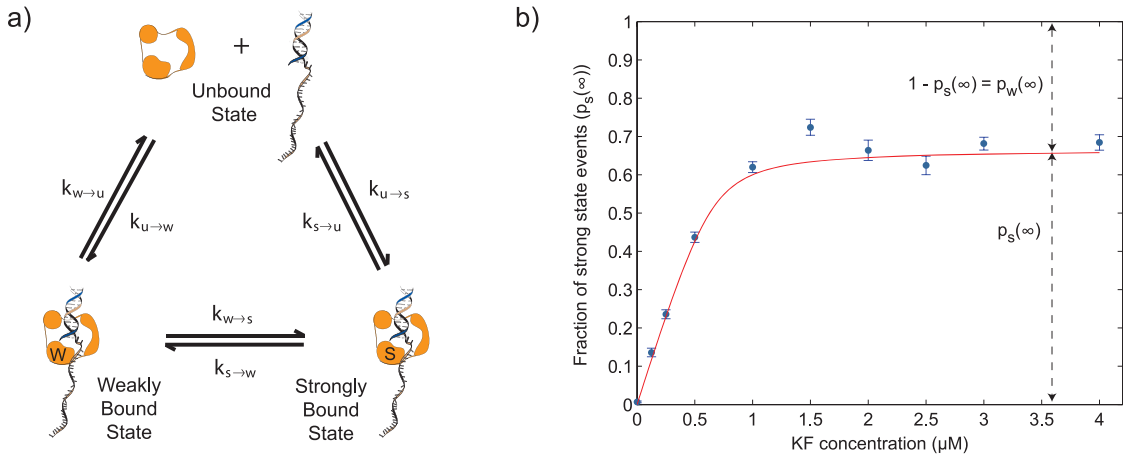

Figure 4. A three-state model is consistent with experimental observations. (a) Diagram of the three states (unbound, weakly bound, strongly bound) with transition rates ($k_{i\to j}$). The "S" and "W" labels on KF are a connotation used in subsequent figures. (b) From capture experiment data (Figure 3a), the measured fraction of strongly bound complexes $p_s(\infty)$ as a function of KF concentration (points) is well modeled by eq 3 (line). At any [KF], the composite fraction $p_u(\infty) + p_w(\infty)$ is $1 - p_s(\infty)$, and at saturating [KF], $p_u(\infty) \approx 0$ and $p_w(\infty) \approx 1 - p_s(\infty)$.

not here resolve the identity of the weak state(s), the implicit existence of this population that is mutually exclusive from the detectable strong state population can be use to model KF−DNA kinetics.

The simplest model that is consistent with experimental observations is a three-state model consisting of unbound, weakly bound, and strongly bound states (Figure 4a). Mathematically, notation is introduced to quantify the kinetics of these states:

$p_u(t)$: the probability of the unbound state at time t,

$p_s(t)$: the probability of the strongly bound state at time t,

$p_w(t)$: the probability of the weakly bound state at time t.

The probabilities are governed by the equations

$$\left.\begin{aligned}\frac{dp_u(t)}{dt} &= -p_u(t)\{k_{u\to w}+k_{u\to s}\}+p_w(t)k_{w\to u}+p_s(t)k_{s\to u}\\ \frac{dp_w(t)}{dt} &= -p_w(t)\{k_{w\to u}+k_{w\to s}\}+p_u(t)k_{u\to w}+p_s(t)k_{s\to w}\\ \frac{dp_s(t)}{dt} &= -p_s(t)\{k_{s\to u}+k_{s\to w}\}+p_u(t)k_{u\to s}+p_w(t)k_{w\to s}\end{aligned}\right\} \quad (1)$$

Our aim is to deduce the six rate constants $k_{i\to j}$, and other model-related parameters, from experimental data. Capture experiments reveal $p_s(t)$ in measurements at each KF concentration, but only at the limiting value $t = \infty$ (*i.e.*, only at equilibrium). The novel active control method (described in Figure 5) permits measurement of *pre-equilbirium* values for $p_s(t)$ at any chosen finite t value. While $p_u(t)$ and $p_w(t)$ cannot be separated in measurements, we do have access to $1 - p_s(t) = p_u(t) + p_w(t)$. Model parameter identification is addressed first based on measurements of $p_s(\infty)$ from capture experiments at varying KF concentrations. Subsequently, the active control method is used to measure $p_s(t)$ at finite t values, followed by modeling the data.

To model capture experiment data, parameters (α,β,K_d) are first defined as

$$\begin{aligned}\alpha &= \frac{[\mathrm{KF}]_{\mathrm{true}}}{[\mathrm{KF}]},\quad \beta = \frac{k_{s\to w}}{k_{w\to s}} = \frac{p_w(\infty)}{p_s(\infty)},\\ K_d &= \frac{p_u(\infty)}{p_w(\infty)+p_s(\infty)}[\mathrm{KF}]_{\mathrm{free}}\end{aligned} \quad (2)$$

The parameter α is introduced as a correction factor that is used to compute the true KF concentration that is competent to bind DNA in the chamber above the nanopore ($[\mathrm{KF}]_{\mathrm{true}}$), given the concentration of KF that is added to the chamber ([KF]) that is based on the activity of the enzyme provided by the supplier. A larger population of KF was anticipated to bind than the population that is competent for synthesis, in which case $\alpha > 1$. The parameter β is the equilibrium constant between the weak and strong states, which is independent of KF concentration. The parameter K_d is the effective binding affinity for the composite KF binding states (weak and strong, together) at equilibrium, with $[\mathrm{KF}]_{\mathrm{free}}$ the concentration of free KF molecules in bulk solution.

The three parameters (α,β,K_d) can be determined from capture experiment data $\{[\mathrm{KF}],p_s(\infty)\}$ as follows. First, we can write $p_u(\infty)$ and $p_w(\infty)$ in terms of β and $p_s(\infty)$, given by $p_w(\infty) = \beta p_s(\infty)$ and $p_u(\infty) = 1 - (\beta + 1)p_s(\infty)$. From these relations and eq 2, $[\mathrm{KF}]_{\mathrm{free}} = K_d(\beta + 1)p_s(\infty)/[1 - (\beta + 1)p_s(\infty)]$. Conservation of the total amount of KF molecules that are competent to bind dictates that

$$\begin{aligned}[\mathrm{KF}]_{\mathrm{true}} &= [\mathrm{DNA}]p_w(\infty)+[\mathrm{DNA}]p_s(\infty)+[\mathrm{KF}]_{\mathrm{free}} \Longrightarrow\\ \alpha[\mathrm{KF}] &= [\mathrm{DNA}](1+\beta)p_s(\infty)+K_d\frac{(\beta+1)p_s(\infty)}{1-(\beta+1)p_s(\infty)}\end{aligned} \quad (3)$$

In eq 3, the added [DNA] is known, and we vary [KF] while measuring $p_s(\infty)$. Equation 3 is reformulated and

maximum likelihood estimation is used to fit (α,β,K_d) to the {[KF],$p_s(\infty)$} data (Supporting Information). The measured data and fitted model (3) are plotted together (Figure 4b), corresponding to the parameter values $\alpha = 1.53 \pm 0.11$, $\beta = 0.50 \pm 0.03$, and $K_d = 69.15 \pm 38.45$ nM. An estimated equilibrium constant between the weak and strong states of β = 50% is consistent with $p_s(\infty) \approx 66\%$ and $p_w(\infty) \approx 33\%$ at saturating [KF]. The value α = 1.5 is larger than we expected, suggesting a 50% increase in KF competent to bind compared to the concentration deemed competent for synthesis by the vendor. Finally, the value $K_d \approx 70$ nM is within the range of 2−200 nM obtained by ensemble measurements.[4]

We next present a method for measuring *pre-steady-state* values for $p_s(t)$, at any chosen finite t value, and for individual DNA−KF molecules. The method combines the nanopore with active control, extending our previous method.[11] Active control refers to automated changes in the voltage across the pore, triggered by time and/or detected shifts in the measured current through the pore. The method here is fully time triggered and involves sequentially and repeatedly exposing the DNA binding site to the bulk-phase *cis*-chamber for a set "fishing period" t_f by a *cis*-positive voltage, followed by a *cis*-negative voltage for 3 ms to probe the state of the DNA (Figure 5). Switching the voltage polarity moves the DNA up or down, while the DNA remains tethered in the nanopore by duplex end regions. The 1−3 ms probing period is sufficient to determine if the DNA is strongly bound or not, based on the current amplitude pattern (Figure 5iii). The first 1 ms of probing is not observable due to capacitances in the system that are excited when the voltage changes polarity (see Methods). The probing voltage used is 120 mV, which is lower than the capture voltage of 180 mV. The lower voltage is used to extend the lifetime of strong state complexes to make a larger percentage of strongly bound complexes observable during the 1−3 ms probing period.

Recorded data sets for each tethered DNA molecule provide two complementary subsets of data. First, we measure $p_s(t_f) \equiv p_s(t_f|p_u(0) = 1)$ for each fishing time t_f chosen by extracting the subset of data that are unbound at the start of fishing (Figure 5iv, left) and computing the fraction of the subset that are subsequently strongly bound at the beginning of probing (Figure 5ii, right). The complementary subset of data corresponds to events that are bound at the start of fishing (Figure 5iv, right), from which we compute the fraction $p_{rb}(t_f) \equiv p_s(t_f|p_s(0) = 1)$ that is subsequently still in the strongly bound state at the start of probing. The subscript rb references that the $p_{rb}(t_f)$ fraction "remains bound" in the sense that the DNA is in the strongly bound state at both the start and the end of each fishing period. It is possible that unbinding and rebinding of the same or a different KF occurred during the fishing period; thus, we are not suggesting that the same KF remains bound for the duration of the entire fishing period for the fraction p_{rb}.

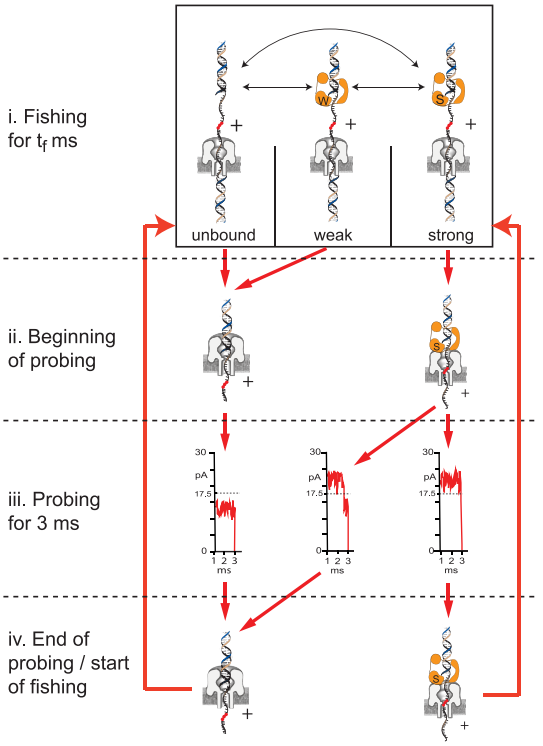

Figure 5. Active control of duplex-tethered DNA in a nanopore to measure pre-steady-state KF−DNA kinetics. (i) Fishing involves exposing the DNA primer-template binding site to the bulk-phase *cis*-chamber by applying a *cis*-positive 50 mV voltage for a set period t_f. During that time, unbound, weak, and strong states can form and interconvert. (ii−iv) Probing begins at the end of the fishing period and applies a *cis*-negative 120 mV voltage for 3 ms. Thus, probing pulls the DNA toward the *trans*-chamber, and during 1−3 ms of probing, the ionic current displays one of three possible patterns as shown in (iii): one pattern consistent with the strong state complex (right signal), one pattern consistent with the unbound state (left signal), and one pattern consistent with the strong state initially followed by the unbound state due to KF dissociation (middle signal). After 3 ms probing, fishing is restarted from one of two possible start states, strong bound or unbound. Automated capture and tethering of each DNA is part of the control logic (see Methods), and hundreds to tens-of-thousands of fish/probe cycles are possible for each tethered DNA (Supporting Information).

The results of measuring $p_s(t_f)$ and $p_{rb}(t_f)$ in separate experiments at [KF] = 0.375 μM (below saturating KF) and [KF] = 2.0 μM (saturating KF), with 1 μM DNA also in the *cis*-chamber, are reported (Figure 6 and Supporting Information Tables S2 and S3) combining data from repeated experiments at each concentration. The trends show $p_s(t_f)$ increasing and $p_{rb}(t_f)$ decreasing as a function of t_f, converging approximately to common equilibrium percentages for each KF concentration. At long fishing times, the fraction of strongly bound events at the start of probing should be at equilibrium, and thus the same fraction should be measured

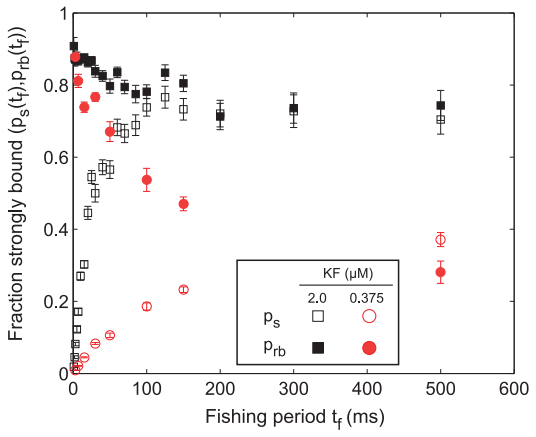

Figure 6. Fraction of strongly bound probing events as a function of fishing period t_f starting from the unbound (p_s) and strongly bound (p_{rb}) states. Regardless of the starting state, the two strongly bound fractions appear to converge to a common equilibrium for long t_f. For short t_f, the observed rate of increase of $p_s(t_f)$ is proportional to KF, shown at saturating (2.0 μM) and subsaturating (0.375 μM) concentrations added to the *cis*-chamber and can be used to identify the association rate parameter $k_{u\to s}$ in (1) at each KF concentration.

regardless of the state of the DNA at the start of fishing. In other words, it should be that $p_{rb}(t_f) \approx p_s(t_f)$ for sufficiently large t_f at each KF concentration, provided the controlled DNA samples KF in the bulk-phase *cis*-chamber in a way that is not biased by the starting state of the DNA (unbound or strongly bound), and this is supported by the data (Figure 6). Also, since the rate of association is proportional to KF concentration, the data show that p_s and p_{rb} converge to equilibrium more quickly at 2.0 μM than at 0.375 μM.

The throughput of our single-molecule-at-a-time method is unparalleled. During a single 2 h experiment, several DNA were captured, tethered, and controlled to generate data for each chosen fishing period. At the fastest fishing period of 1 ms, each fishing/probing cycle lasts 4 ms (3 ms probing and 1 ms fishing). In one of the experiments at 2.0 μM KF, at total of 14 797 cycles were recorded at the 1 ms fishing period, which corresponds to just under 60 s of recording time. For each fishing time, hundreds to tens-of-thousands of single-molecule events were recorded, one molecular event at a time. In total, over 200 000 fishing/probing cycles were included in the 2.0 μM KF data plotted in Figure 6; this is 2 orders of magnitude more events than is recorded in a typical nanopore capture experiment. We know of no other single-molecule method that can generate as much data in as short a time period. By contrast, single-molecule FRET measures individual molecules that are each labeled, but the measurements are images that record all fluorescent signals generated in parallel within the image frame. Optical trapping and AMF setups can measure one molecule at a time, and while each measurement is considerably more informative (such as tracking a motor for hundreds of steps along polynucleotide substrate[15]), the throughput is considerably lower.

Finally, based on the data generated in fishing/probing experiments, we examine the unbound-to-strong association rate ($k_{u\to s}$) in the three-state model illustrated in Figure 4. In each event, the dsDNA–ssDNA junction is first sent into the bulk-phase *cis*-chamber for a prescribed fishing period of t_f, and then the voltage is reversed to pull the DNA back against the pore to probe if a KF molecule is bound onto the DNA in the strong state. After 3 ms probing, the voltage is reversed again to start the next fishing event. To estimate $k_{u\to s}$, we select only fishing events that start with the DNA in the unbound state ($p_s(t)$). Mathematically, over the ensemble of all events we select, we have $p_u(0) = 1$, $p_w(0) = 0$, and $p_s(0) = 0$. Substituting into eq 1, we obtain

$$\left.\frac{dp_s(t)}{dt}\right|_{t=0} = k_{u\to s}$$

Thus, $k_{u\to s}$ is the initial rate of change in $p_s(t)$. In Figure 7a, we plot p_s *versus* t_f measured at various KF concentrations. The data confirm that $p_s(t_f)$ is indeed proportional to t_f for small t_f. At each KF concentration, $k_{u\to s}$ is calculated as the slope of $p_s(t_f)$ (Tables S4 and S5). The plot of $k_{u\to s}$ *versus* [KF] is shown in Figure 7b. Data points of $k_{u\to s}$ are fitted using the least-squares method to, respectively, $k_{u\to s} \propto [KF]$ and $k_{u\to s} \propto [KF]_{free}$. The plot suggests that the association rate $k_{u\to s}$ is approximately proportional to [KF], the total (unbound and DNA-bound) KF concentration added to the *cis*-chamber. The least-squares fitting yields $k_{u\to s} \approx 10.6\ s^{-1}\ \mu M^{-1}[KF]$ (solid line in Figure 7b)). In contrast, the model $k_{u\to s} \propto [KF]_{free}$ (dashed line in Figure 7b)) cannot explain the measured values of $k_{u\to s}$.

CONCLUSIONS

Our work models pre-equilibrium kinetics between the KF and DNA substrate, based on analyzing capture event measurements from standard nanopore experiments and also using our new active control method for measuring association and dissociation of individual KF from a single DNA duplex tethered in the nanopore. Ours is the first nanopore study to examine *unforced* dissociation between each KF and the controlled DNA, a measurement made implicitly available only through the control method itself. This study is also the first to show that KF–DNA complexes captured on the pore are not universally detectable. The detectable binding state is shown to sample the open configuration and to measurably respond to dNTP incorporation and subsequently sample the closed ternary complex, as shown in other nanopore studies.[9] Moreover, the undetectable KF–DNA complexes

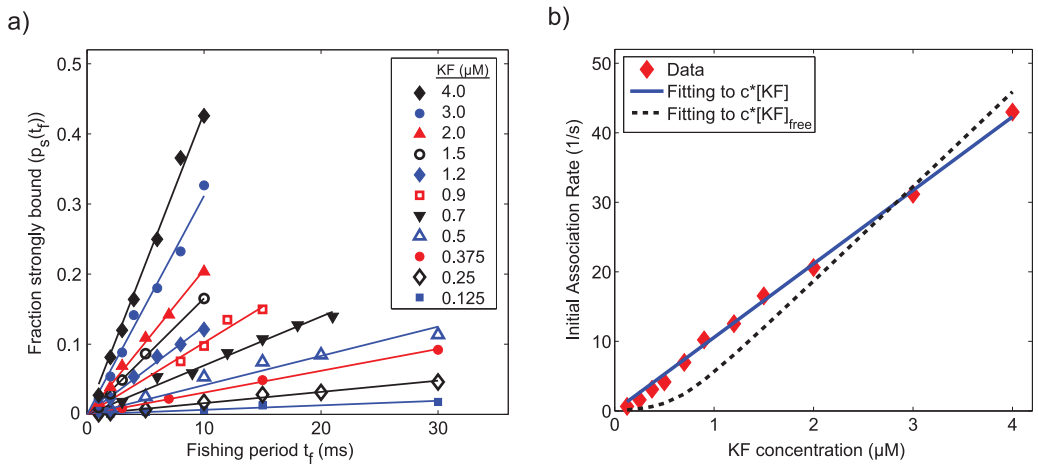

Figure 7. Results of fishing experiments that start with the DNA in the unbound state. (a) Fraction of strongly bound events (p_s) over short fishing periods t_f at various KF concentrations. For all KF concentrations used in experiments, fraction of strongly bound (p_s) increases linearly with fishing period for small t_f. Each solid line represents the linear fitting at a KF concentration. The slope of each line gives the unbound-to-strong association rate (the transition rate $k_{u\to s}$) at the corresponding KF concentration. (b) Unbound-to-strong association rate (the slope of p_s *vs* t_f in panel a) as a function of KF concentration. The solid line shows the fitting to c[KF], whereas the dashed line is the fitting to $c[KF]_{free}$, where $[KF]_{free}$ is the free KF concentration in solution. It is clear that the association rate is not proportional to $[KF]_{free}$.

captured on the nanopore are mutually exclusive from the detectable binding state. Though we are not able to resolve the configuration that corresponds to undetectable binary events, varying experimental conditions support that the state is not an artifact of the measurement technique but is intrinsic to the KF–DNA complexes captured on the nanopore. Using the active control method, our study also complements prior nanopore studies on KF–DNA kinetics[9,10] by measuring and quantifying the rates of formation of binary complexes. An unexpected result is that the measured association rate of KF to the controlled DNA cannot be explained by the model of association rate being proportional to free KF concentration. Instead, the measured association rate is approximately proportional to the total (unbound and DNA-bound) KF concentration in the chamber above the pore. The molecular mechanism for this phenomenological observation is still unknown. One possibility is that, when a unbound DNA encounters a DNA with a KF molecule bound, the KF molecule can somehow transfer from one DNA to the other. Future experiments need to be designed to test this hypothesis.

The DNA control method presented here is simple to implement on any nanopore experiment setup, with dedicated hardware that is commercially available. The method here is a fully time-triggered two-cycle logic (probe, then fish), which makes the logic very simple to program and implement. The throughput of this method is unparalleled, recording hundreds-of-thousands of single-molecule events in a few hours, one molecular event at a time. A distinct feature is that the method allowed us to measure two conditional probabilities for the strongly bound complex in repeated fishing events with the same DNA molecule that is tethered at the pore: one starting in the unbound state, and the other starting in the strong bound state at the onset of fishing. Another advantage is that, upon the capture of one DNA, it uses the captured DNA repeatedly for a large number of fishing events (over 10 000 per DNA in some cases). Thus, a slow capture rate caused by low DNA concentration will not impact the high-throughput dramatically. Being able to work with low DNA concentration will enable us, in particular, to distinguish the effect of DNA-bound KF molecules in bulk from that of free KF molecules in bulk on the transition rate from unbound to strongly bound. The demonstrated control technique is not confined to the study of KF with DNA but could be applied to other DNA or RNA-binding enzymes that are conducive to nanopore experimental conditions. Notably, enzymes that function in higher salt can be measured at lower probing forces (as in ref 10), making it more likely to detect complexes that would not survive the higher nanopore contact forces experienced in capture experiments.

The ability to quickly quantitate, even grossly, the kinetics of protein binding to nucleic acids, whether it be dsDNA, ssDNA, or RNA, has significant relevance to the biotechnology industry. For example, it is advantageous to re-engineer proteins to bind methylated DNA with higher affinity and greater sequence specificity to enable mapping regions of hyper-methylated DNA, which are common DNA "marks" in cancers and other disease states.[16,17] It is also common practice to investigate binding kinetics when developing novel DNA binding enzymes used in commercial molecular biology kits.[18] The method discussed in this article offers a convenient strategy to quickly screen proteins and determine whether sequence modifications, either protein or DNA, have increased or decreased

the proteins' affinity for its target. Additionally, the method can be amended to determine the affinity of bacterial or viral proteins for nucleic acids in the presence of small molecule drug candidates. For example, by using a segment of RNA that matches the Hepatitis C genome and the Hepatitis C RNA binding replicase protein in the bulk phase, one could screen small-molecule inhibitors that prevent enzyme association with the RNA, thereby realizing hits for potential compounds for treating Hepatitis C infection.

METHODS

Materials. The D355A,E357A exonuclease-deficient variant of KF was obtained from New England Biolabs (100 000 U mL^{-1}; specific activity 20 000 U mg^{-1}). DNA oligonucleotides were synthesized by the Stanford University Protein and Nucleic Acid Facility and purified by denaturing PAGE. Sequences of the oligonucleotides used in this study are shown below. The abasic residues in the 79-mer template sequence are indicated by an X. The 3′ terminal residue of the 23-mer primer was 2′-3′ dideoxycytidine (ddC), enabling binary and ternary complex formation without catalytic turnover. 23-mer primer: 5′-GGCTACGACCTGCATGAGAATGddC-3′. 20-mer tethering oligonucleotide: 5′-TGAGTGGAAGGATAGGTGAG-3′. Three abasic (**XXX**) residue-containing 79-mer template: 5′-CTCACCTATCCTTCCACTCATTCCAATTAATTACCATTCATT**XXX**TCTCACTATCGCATTCTCATGCAGGTCGTAGCC-3′.

General Nanopore Methods. Experiments were conducted at 23 °C in 10 mM HEPES/KOH, pH 8.00 ± 0.05, 0.3 M KCl, 5 mM $MgCl_2$, which are conditions shown to support KF catalytic function.[8,9] Single α-HL channels were formed as described.[8] A patch-clamp amplifier (AxoPatch 200B, Molecular Devices, Sunnyvale, CA) was used to apply transmembrane voltage and measure ionic current, with the 4-pole Bessel filter set at 5 kHz bandwidth. A digitizer (Digidata 1440A, Molecular Devices) stored data sampled at 100 or 200 kHz. Primer/template hybrids were formed by mixing in equimolar concentrations of 50 μM each in a solution containing 100 mM KCl and 5 mM $MgCl_2$. The solution was denatured at 95 °C for 2 min, followed by a slow cool to room temperature to optimize annealing specificity. This solution was then added at a concentration of 1 μM into the *cis*-chamber during nanopore experiments. Tethering primer was present in the *trans*-chamber at a concentration of 4 μM. Standardization of *cis*-chamber volume to 85 μL was performed after insertion of a single nanopore into the lipid bilayer and after flushing excess α-HL from the nanopore. Evaporation of water from the nanopore setup was prevented by saturating the humidity level directly above the nanopore device.

Active Voltage Control Experiments. Active voltage control logic was implemented as a finite state machine (FSM) on a field-programmable gate array (FPGA, PCI-7831R, National Instruments), as described previously.[11] The FPGA was connected to the Axopatch 200B for transmembrane voltage control and ionic current measurements at 5.3 μs updates. To improve the signal-to-noise ratio, the ionic current signal was filtered on the FPGA using a single-pole low-pass filter with 1.58 kHz cutoff frequency. The FSM initialized tethering by detecting capture of a primer-template DNA molecule at 160 mV and reducing the voltage to 50 mV for 10 s. The holding period permits *trans*-side duplex formation (20 bp) between the 20 nucleotides of the template exposed in the *trans*-chamber (from 5′ end) and the 20-mer tethering oligonucleotide with high likelihood.[11] The FSM then began automated cycling between the −20 mV fishing voltage for each chosen fishing period t_f specified in results section with the 120 mV probing voltage for 3 ms. The logic looped continuously between fishing and probing voltages until the FSM detected an open channel current level during probing, which triggered a return to 160 mV capture voltage until detection of capture of another DNA molecule. Testing for open channel current was at the end of each probing period to avoid the effect of the capacitive transient on the sensing signal.

Data Processing. All numerical analysis and data processing was done using custom code written in Matlab (20011a, The MathWorks, Natick, MA). Analysis of capture event data was done with methods established in prior work.[8,11] Analysis of active control (fishing/probing) data was done with methods comparable to our prior work in ref 11, with modifications to uniquely identify each of the three signal patterns (Figure 5iii) during each 3 ms probing period. In nanopore systems using patch-clamp technology, a step change in voltage induces a capacitive transient superimposed on the ionic current measurement. To remove the current transient induced by the voltage change that initiates each 3 ms probing period, a simple exponential subtraction method was used offline (as done in ref 10). Briefly, a one-time transient fit was made using one probing event for each tethered DNA molecule, and the fit was subtracted for all probing events for that molecule. In the transient fit, the first 0.2 ms of the current is saturated and ignored in the data, and a three-parameter exponential function $f(t) = a_0 + a_1 \exp(-a_3 t)$ was fit in Matlab using a built-in nonlinear least-squares to determine parameters a_0, a_1, a_2. Subtraction of the resulting fit $a_1 \exp(-a_3 t)$ for each probing period yielded events with steady-state amplitudes achieved 1 ms after the start of probing (as shown in Figure 5iii). Each of the three signal patterns (Figure 5iii) were subsequently identified using the step detection method in ref 11. The threshold in step detection was based on the observed amplitude separation between strongly bound and unbound DNA event amplitudes at 120 mV and was calibrated for each experiment. Any step signaling the transition from strongly bound to unbound (middle pattern, Figure 5iii) that occurred within the first millisecond of probing was therefore not detected. To compensate for this, we apply the same correction factor method used to adjust the strongly bound percentage in capture experiments (Supporting Information). The correction increases the fraction of strongly bound probing events by a factor of 1.1, with the corrected percentages plotted in Figure 6 (uncorrected data are reported in Tables S2 and S3).

Conflict of Interest: The authors declare no competing financial interest.

Acknowledgment. This work was supported by National Institutes of Health Grants HG004035-05 (W.D.) and R21-RR025347-02 (H.W., W.D.). We thank J. Dahl for repeating some of the capture experiments, and K. Lieberman for proposing experiments and providing feedback on aspects of this work. We also thank T. Morin for helpful editing and suggesting potential applications for our method.

Supporting Information Available: (1) DNA primer/template substrate (Figure S1). (2) Selection criteria for assigning type A/type B events (Figure S2). (3) Correction factor for the fraction of type B events (Figure S3). (4) Capture rate of DNA without and with saturating KF (Figure S4). (5) Fraction of type B events under varying experimental conditions (Figure S5, Table S1). (6) Fitting capture data parameters by maximum likelihood estimation. (7) Fishing/probing data (Tables S2 and S3). (8) Correction factor for the fraction of strongly bound probing events in fishing/probing data. (9) Rate of association data from fishing/probing experiments (Tables S4 and S5). This material is available free of charge *via* the Internet at http://pubs.acs.org.

REFERENCES AND NOTES

1. Rothwell, P. J.; Waksman, G. Structure and Mechanism of DNA Polymerases. *Adv. Protein Chem.* **2005**, *71*, 401–440.

2. Joyce, C. M.; Benkovic, S. J. DNA Polymerase Fidelity: Kinetics, Structure, and Checkpoints. *Biochemistry* **2004**, *43*, 14317–14324.
3. Astatke, M.; Grindley, N. D.; Joyce, C. M. How *E. coli* DNA Polymerase I (Klenow Fragment) Distinguishes between Deoxy- and Dideoxynucleotides. *J. Mol. Biol.* **1998**, *278*, 147–165.
4. Kuchta, R. D.; Mizrahi, V.; Benkovic, P. A.; Johnson, K. A.; Benkovic, S. J. Kinetic Mechanism of DNA Polymerase I (Klenow). *Biochemistry* **1987**, *26*, 8410–8417.
5. Bermek, O.; Grindley, N. D. F.; Joyce, C. M. Distinct Roles of the Active-Site Mg^{2+} Ligands, Asp882 and Asp705, of DNA Polymerase I (Klenow Fragment) during the Prechemistry Conformational Transitions. *J. Biol. Chem.* **2011**, *286*, 3755–3766.
6. Joyce, C. M.; Potapova, O.; Delucia, A. M.; Huang, X.; Basu, V. P.; Grindley, N. D. F. Fingers-Closing and Other Rapid Conformational Changes in DNA Polymerase I (Klenow Fragment) and Their Role in Nucleotide Selectivity. *Biochemistry* **2008**, *47*, 6103–6116.
7. Santoso, Y.; Joyce, C. M.; Potapova, O.; Le Reste, L.; Hohlbein, J.; Torella, J. P.; Grindley, N. D. F.; Kapanidis, A. N. Conformational Transitions in DNA Polymerase I Revealed by Single-Molecule FRET. *Proc. Natl. Acad. Sci. U.S.A.* **2010**, *107*, 715–720.
8. Benner, S.; Chen, R. J.; Wilson, N. A.; Abu-Shumays, R.; Hurt, N.; Lieberman, K. R.; Deamer, D. W.; Dunbar, W. B.; Akeson, M. Sequence-Specific Detection of Individual DNA Polymerase Complexes in Real Time Using a Nanopore. *Nat. Nanotechnol.* **2007**, *2*, 718–724.
9. Hurt, N.; Wang, H.; Akeson, M.; Lieberman, K. R. Specific Nucleotide Binding and Rebinding to Individual DNA Polymerase Complexes Captured On a Nanopore. *J. Am. Chem. Soc.* **2009**, *131*, 3772–3778.
10. Garalde, D. R.; Simon, C. A.; Dahl, J. M.; Wang, H.; Akeson, M.; Lieberman, K. R. Distinct Complexes of DNA Polymerase I (Klenow Fragment) for Base and Sugar Discrimination during Nucleotide Substrate Selection. *J. Biol. Chem.* **2011**, *286*, 14480–14492.
11. Wilson, N. A.; Abu-Shumays, R.; Gyarfas, B.; Wang, H.; Lieberman, K. R.; Akeson, M.; Dunbar, W. B. Electronic Control of DNA Polymerase Binding and Unbinding to Single DNA Molecules. *ACS Nano* **2009**, *3*, 995–1003.
12. Venkatesan, B.; Bashir, R. Nanopore Sensors for Nucleic Acid Analysis. *Nat. Nanotechnol.* **2011**, *6*, 615–624.
13. Song, L.; Hobaugh, M. R.; Shustak, C.; Cheley, S.; Bayley, H.; Gouaux, J. E. Structure of Staphylococcal α-Hemolysin, a Heptameric Transmembrane Pore. *Science* **1996**, *274*, 1859–1866.
14. Guest, C. R.; Hochstrasser, R. A.; Dupuy, C. G.; Allen, D. J.; Benkovic, S. J.; Millar, D. P. Interaction of DNA with the Klenow Fragment of DNA Polymerase I Studied by Time-Resolved Fluorescence Spectroscopy. *Biochemistry* **1991**, *30*, 8759–8770.
15. Moffitt, J. R.; Chemla, Y. R.; Smith, S.; Bustamante, C. Recent Advances in Optical Tweezers. *Annu. Rev. Biochem.* **2008**, *77*, 205–228.
16. Jørgensen, H. F.; Adie, K.; Chaubert, P.; Bird, A. P. Engineering a High-Affinity Methyl-CpG-Binding Protein. *Nucleic Acids Res.* **2006**, *34*, e96.
17. Shim, J.; Humphreys, G. I.; Venkatesan, B. M.; Munz, J. M.; Zou, X.; Sathe, C.; Schulten, K.; Kosari, F.; Nardulli, A. M.; Vasmatzis, G.; Bashir, R. Detection and Quantification of Methylation in DNA Using Solid-State Nanopores. *Sci. Rep.* **2013**, *3*, 1–8.
18. Buchholz, F. Engineering DNA Processing Enzymes for the Postgenomic Era. *Curr. Opin. Biotechnol.* **2009**, *20*, 383–389.